JOURNAL OF VIROLOGY, Sept. 2010, p. 8460–8469 Vol. 84, No. 17
0022-538X/10/$12.00 doi:10.1128/JVI.00902-10

Visualizing the Replication Cycle of Bunyamwera Orthobunyavirus Expressing Fluorescent Protein-Tagged Gc Glycoprotein▽†

Xiaohong Shi, Joël T. van Mierlo,‡ Andrew French,§ and Richard M. Elliott*

Centre for Biomolecular Sciences, School of Biology, University of St. Andrews, North Haugh, St. Andrews, KY16 9ST Scotland, United Kingdom

Received 27 April 2010/Accepted 13 June 2010

The virion glycoproteins Gn and Gc of Bunyamwera virus (BUNV), the prototype of the *Bunyaviridae* family and also of the *Orthobunyavirus* genus, are encoded by the medium (M) RNA genome segment and are involved in both viral attachment and entry. After their synthesis Gn and Gc form a heterodimer in the endoplasmic reticulum (ER) and transit to the Golgi compartment for virus assembly. The N-terminal half of the Gc ectodomain was previously shown to be dispensable for virus replication in cell culture (X. Shi, J. Goli, G. Clark, K. Brauburger, and R. M. Elliott, J. Gen. Virol. 90:2483–2492, 2009.). In this study, the coding sequence for a fluorescent protein, either enhanced green fluorescent protein (eGFP) or mCherry fluorescent protein, was fused to the N terminus of truncated Gc, and two recombinant BUNVs (rBUNGc-eGFP and rBUNGc-mCherry) were rescued by reverse genetics. The recombinant viruses showed bright autofluorescence under UV light and were competent for replication in various mammalian cell lines. rBUNGc-mCherry was completely stable over 10 passages, whereas internal, in-frame deletions occurred in the chimeric Gc-eGFP protein of rBUNGc-eGFP, resulting in loss of fluorescence between passages 5 and 7. Autofluorescence of the recombinant viruses allowed visualization of different stages of the infection cycle, including virus attachment to the cell surface, budding of virus particles in Golgi membranes, and virus-induced morphological changes to the Golgi compartment at later stages of infection. The fluorescent protein-tagged viruses will be valuable reagents for live-cell imaging studies to investigate virus entry, budding, and morphogenesis in real time.

Bunyamwera virus (BUNV) is the prototype of both the family *Bunyaviridae* and the genus *Orthobunyavirus*. The characteristic features shared by all viruses in the family (known as bunyaviruses) include spherical virion morphology, possession of a tripartite, single-stranded RNA genome of negative or ambisense polarity, cytoplasmic site of virus replication, and assembly and budding of progeny particles at membranes of the Golgi complex (6, 27). The family includes a number of significant human pathogens such as La Crosse virus (LACV), Hantaan virus (HTNV), Sin Nombre virus (SNV), Rift Valley fever virus (RVFV), and Crimean-Congo hemorrhagic fever virus (CCHFV) (7). All bunyaviruses encode four structural proteins, two surface glycoproteins called Gn and Gc, and two internal proteins, N (nucleocapsid protein that encapsidates the genomic RNA segments) and L (RNA-dependent RNA polymerase). In addition, the majority of bunyaviruses also encode nonstructural proteins. The sizes of the viral proteins vary considerably across the family though they are relatively well conserved between viruses within a particular genus. The glycoproteins form spikes on the virion surface and are involved in viral attachment and cell fusion (35). They are encoded by the medium (M) RNA genome segment as a polyprotein precursor (Gn at the N terminus and Gc at the C terminus) that is cleaved cotranslationally to yield the mature virion glycoproteins. Both glycoproteins are type I integral transmembrane (TM) proteins and are modified by N-linked glycosylation. Gn and Gc form a heterodimer in the endoplasmic reticulum (ER) prior to trafficking and retention in the Golgi compartment for virus assembly (31, 35). The BUNV M segment additionally encodes a nonstructural protein termed NSm that is sandwiched between Gn and Gc (19). BUNV NSm is also an integral membrane protein, and the N-terminal domain, at least, of NSm is required for virus assembly (42). BUNV Gn is able to target to the Golgi complex alone, whereas correct folding, maturation, and Golgi complex targeting of the Gc protein depends on the chaperone-like assistance of Gn (18, 38, 44).

The BUNV Gn protein consists of 302 residues with a rather long predicted cytoplasmic tail (CT) of 78 residues, while the larger Gc protein comprises 957 residues with a CT of only 25 residues (Fig. 1) (8, 19). The CT domains of both Gn and Gc play crucial roles in BUNV-mediated membrane fusion, virus assembly, and morphogenesis (43). Functional analysis of deletion mutants of BUNV Gc indicated that nearly half of its N-terminal ectodomain (453 residues out of 909 residues) is dispensable for Golgi trafficking, cell fusion, and virus replication in cell culture (41). Similarly, characterization of mutants of the related Maguari virus (MAGV) also showed that the N-terminal domain of Gc was not essential for growth in cell culture (33). These data suggested that it might be possible to insert foreign sequences, e.g., those encoding an autofluores-

* Corresponding author. Mailing address: Centre for Biomolecular Sciences, School of Biology, University of St. Andrews, North Haugh, St. Andrews, KY16 9ST Scotland, United Kingdom. Phone: 44 1334 463396. Fax: 44 1334 462595. E-mail: rme1@st-andrews.ac.uk.

‡ Present address: Department of Medical Microbiology, Nijmegen Centre for Molecular Life Sciences, Radboud University Nijmegen Medical Centre, P.O. Box 9101, 6500 HB Nijmegen, Netherlands.

§ Present address: The Scottish Institute for Cell Signalling, The Sir James Black Centre, College of Life Sciences, University of Dundee, Dow Street, Dundee DD1 5EH, Scotland, United Kingdom.

† Supplemental material for this article may be found at http://jvi.asm.org/.

▽ Published ahead of print on 23 June 2010.

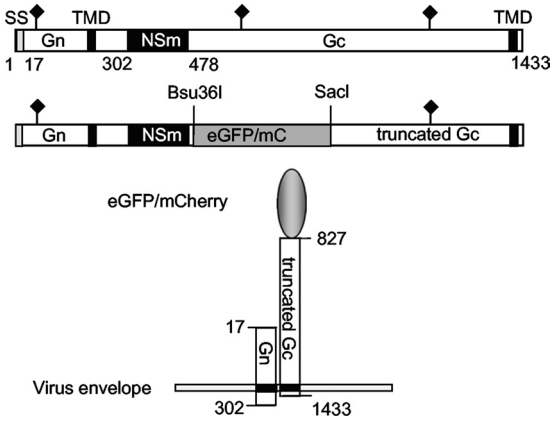

FIG. 1. Schematic diagrams of eGFP- and mCherry-tagged BUNV glycoproteins. The layout of the wt BUNV glycoprotein precursor (Gn, NSm, and Gc) is shown at the top, with positions of amino acid residues marking the protein boundaries indicated. Below is shown the structure of the chimeric Gc protein, with substitution of the N terminus of Gc (residues 500 to 826) with the coding sequence of either enhanced green fluorescent protein (eGFP) or mCherry fluorescent protein (mC) attached to truncated Gc. The predicted topology of Gn and eGFP/mCherry-tagged Gc on the viral envelope is shown at the bottom. SS, signal peptide; TMD, transmembrane domain. The filled diamonds indicate glycosylation sites.

cent protein, in place of the N-terminal domain to generate recombinant viruses expressing a tagged Gc protein (41).

In this paper we report the successful insertion of the coding region of either the enhanced green fluorescent protein (eGFP) or mCherry red fluorescent protein into the BUNV glycoprotein precursor to replace the dispensable region at the N terminus of the Gc ectodomain. Viable viruses with Gc tagged by either eGFP or mCherry were rescued by reverse genetics, and fluorescent extracellular virions were detectable by conventional fluorescence or confocal microscopy. The processes of virus attachment and internalization and budding of progeny virions could be visualized in infected cells.

MATERIALS AND METHODS

Cells and viruses. BHK-21 and BSR-T7/5 (4) cells were maintained in Glasgow minimal essential medium (GMEM; Invitrogen) supplemented with 10% tryptose phosphate broth, 10% fetal calf serum, and, for BSR-T7/5 cells only, 1 mg of Geneticin (G418) sulfate (Calbiochem) per ml, as described previously (22, 44). A549 cells and Vero E6 (ATCC C1008) cells were grown in Dulbecco's modified Eagle's medium (Invitrogen) supplemented with 10% fetal calf serum. Stocks of wild-type (wt) and recombinant BUNV (rBUNV) were plaque purified in BHK-21 cells. Working stocks were grown by infecting BHK-21 cells in a 175-cm^2 flask with 500 μl of elite stock and harvesting the supernatant when extensive cytopathic effect (CPE) was apparent.

Titers of the working stocks were determined by plaque assay as previously described (48).

Antibodies. Rabbit antisera against BUNV particles (anti-BUN) and BUNV N protein (anti-N) and mouse monoclonal antibody (MAb) 742 against BUNV Gc protein were described previously (18, 49). MAbs against GM130, a Golgi matrix protein, were purchased from BD Bioscience; MAbs against α-tubulin (CP06) were from Calbiochem, and those against eGFP (ab1218) were from Abcam. Goat anti-rabbit antibody conjugated with fluorescein isothiocyanate (FITC) was purchased from Sigma, and goat anti-mouse antibody conjugated with Cy5 was purchased from Chemicon International Inc.

Plasmids. Plasmids that generate full-length BUNV antigenome RNA transcripts [pT7riboBUNL(+), pT7riboBUNM(+), and pT7riboBUNS(+)] have been described previously (3, 22). pT7riboBUNMGc-eGFP and pT7riboBUNMGc-mCherry were constructed by replacing the coding region for residues 501 to 826 of the glycoprotein precursor in pT7riboBUNM(+) with that of either eGFP (11) or mCherry red protein (36). pT7riboBUNM(+) was first modified to introduce a unique SacI restriction site at nucleotide (nt) 2534 of the cDNA by PCR mutagenesis. The coding regions for eGFP and mCherry were amplified by PCR from plasmids pEGFP-N1 and pmCherry (both Clontech Laboratories), with the introduction of Bsu36I and SacI restriction enzyme sites at the 5′ and 3′ ends. The DNA products were ligated into modified pT7riboBUNM(+) that had been digested with Bsu36I (site at nt 1549 in the BUNV M segment cDNA) and SacI (Fig. 1). All constructs were confirmed by DNA sequence analysis. The primers used and details of PCR are available upon request.

Virus rescue by reverse genetics and virus growth curves. Rescue experiments were performed essentially as described previously (22). Briefly, BSR-T7/5 cells were transfected with a mixture of plasmids comprising 1.0 μg each of pT7riboBUNL(+), pT7riboBUNS(+), and either pT7riboBUNMGc-eGFP or pT7riboBUNMGc-mCherry. At 5 h posttransfection, 4 ml of growth medium was added, and incubation continued for 5 to 11 days at 33°C. The expression of either eGFP- or mCherry-tagged Gc proteins by the transfectant viruses (rBUNGc-eGFP and rBUNGc-mCherry, respectively) was initially examined under a fluorescence microscope, and plaques were isolated on BHK-21 cells. Elite virus stocks were produced by infecting BHK-21 cells in a 25-cm^2 flask with a single plaque and growing the cultures at 33°C until CPE was evident. To monitor virus growth, BHK-21 cells in 35-mm-diameter petri dishes were infected at a multiplicity of infection (MOI) of 0.1 PFU per cell, and supernatants were harvested at various times after infection. Virus titers were determined by plaque formation on BHK-21 cells.

Metabolic radiolabeling, immunoprecipitation, and Western blotting. Procedures for metabolic radiolabeling and immunoprecipitation of BUNV proteins were described previously (39). Briefly, at 24 h postinfection (p.i.), cells were labeled with [^{35}S]methionine (80 μCi) for 1 h and then lysed, on ice, in 300 μl of nondenaturing radioimmunoprecipitation assay (RIPA) buffer (50 mM Tris-HCl [pH 7.4], 1% Triton X-100, 300 mM NaCl, 5 mM EDTA) containing a cocktail of protease inhibitors (Roche). BUNV glycoproteins were immunoprecipitated with anti-BUN serum that had been conjugated to protein A-Sepharose (Sigma) and were analyzed by SDS-PAGE under reducing conditions. For Western blotting, cell lysates of infected BHK-21 cells were separated on 4 to 12% gradient polyacrylamide NuPAGE gels (Invitrogen) and transferred onto a polyvinylidene difluoride (PVDF) membrane (Millipore). The membrane was reacted with appropriate antibodies, and signals were detected by chemiluminescence as described previously (20).

PNGase F digestion. Immunoprecipitates of infected cells were denatured in 30 μl of denaturing buffer (0.5% SDS and 1% β-mercaptoethanol) at 100°C for 10 min and cooled to room temperature. The samples were digested with 4 mU of peptide N-glycosidase F (PNGase F; New England Biolabs) in 40 μl of reaction buffer (50 mM sodium phosphate [pH 7.5], 0.5% SDS, 1% β-mercaptoethanol) for 20 h at 37°C. Treated samples were analyzed by SDS-PAGE.

Immunofluorescence and live-cell imaging of eGFP/mCherry-tagged BUNV infection. To examine the autofluorescence of recombinant virus particles, 5 μl of infectious supernatant, clarified by centrifugation at 3,000 × *g* for 5 min to remove cellular debris, was mixed with 5 μl of Mowiol mounting medium (pH 8.5) and examined using a Deltavision 3.5 image restoration microscope (Applied Precision). Observations of virus-infected cells by immunofluorescence were as described previously (40). Briefly, infected cells were fixed with 4% paraformaldehyde and then permeabilized with 0.1% Triton X-100 in phosphate-buffered saline (PBS) before they were costained with specific primary antibodies and secondary antibody conjugates. Localization of fluorescently labeled proteins was examined using either the Deltavision 3.5 restoration microscope or a Zeiss LSM confocal microscope as described in the figure legends. For three dimensional (3D) reconstructions of virus-infected cells, a series of images was captured on the Deltavision microscope with *Z*-sections of 0.2 μm across the cell. Deconvolution and surface rendering for tertiary reconstruction were processed by Huygens Deconvolution software, version 3.4 (Scientific Volume Imaging).

For live-cell imaging, BHK-21 cells grown on chamber slides (μ-Slide with eight wells; ibidi Gmbh, Munich, Germany) and maintained in CO_2-independent medium (Invitrogen), were infected with rBUNGc-eGFP at an MOI of 0.05 PFU/cell. From 12 h postinfection the images were collected at 10-min interval with a *Z*-section setting of 1 μm (11 images from top to bottom of cell). The *Z*-stacked images and video clip were processed using Huygens Deconvolution software.

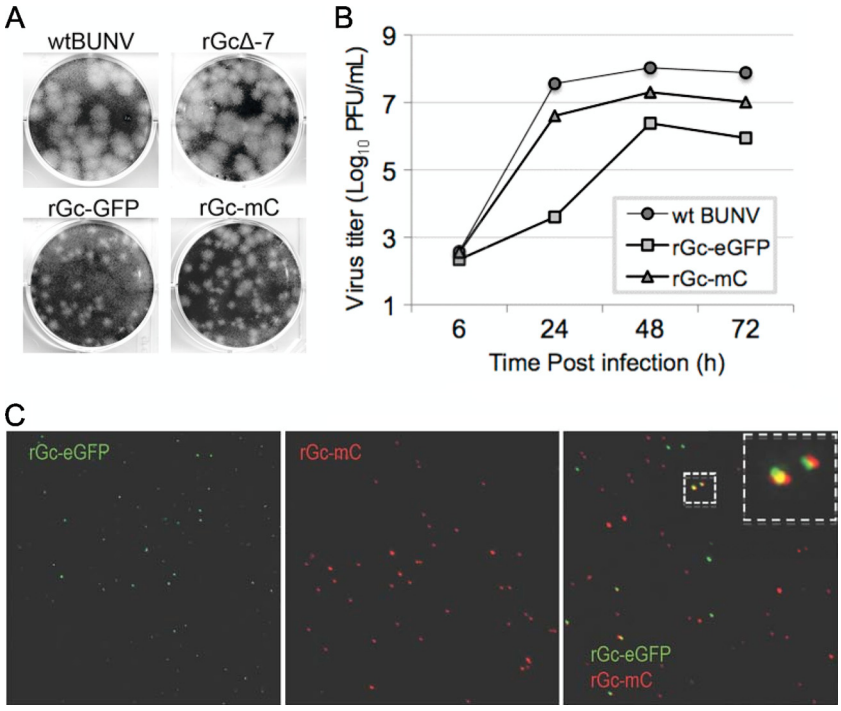

FIG. 2. Plaque morphology, growth kinetics, and autofluorescence of recombinant viruses. (A) Comparison of the plaque sizes on BHK-21 cells. Cells were fixed at 6 days postinfection with 4% formaldehyde and stained with Giemsa solution. (B) Virus growth curves on BHK-21 cells at 33°C. Cells were infected with wt BUNV virus or the rBUNGc-eGFP (rGc-eGFP) or rBUNGc-mCherry (rGc-mC) recombinant virus at an MOI of 0.1 PFU/cell. Virus was harvested at the indicated times after infection and titrated by plaque formation on BHK-21 cells. Results are shown as the mean of the duplicate titrations. (C) Autofluorescence of recombinant viruses. The supernatant from infected cells containing released virus particles was mixed with an equal volume of Mowiol mounting medium and observed in the Deltavision microscope. Left and middle panels show the autofluorescence of rBUNGc-eGFP (green) and rBUNGc-mCherry (red) viruses, and the right panel shows the image when green and red viruses were mixed. The enlarged inset shows aggregates of green and red viruses. rGcΔ-7, rBUNGcΔ7.

RESULTS

Generation of recombinant BUNV containing Gc tagged with eGFP or mCherry. Recently, we reported a functional analysis of the BUNV Gc protein and observed that the N-terminal half of the Gc ectodomain (residues 477 to 930 of the precursor polyprotein), which forms two structural domains, was not essential for virus replication in cell culture (41). We created four viruses by reverse genetics carrying deletions in Gc ranging from 218 to 450 amino acids, and while all recombinants were attenuated in cell culture, the virus designated rBUNGcΔ7 that lacked amino acids 480 to 826 of the precursor was the least impaired. Hence, we used this deletion as the basis to insert a foreign protein that would be expressed on the surface of recombinant BUNV particles (41). To facilitate cloning of the foreign gene, we introduced a unique SacI restriction enzyme site at nt 2534 in the BUNV M segment cDNA and made use of the naturally occurring Bsu36I site at position 1549. This would allow replacement of amino acids 501 to 826 of the glycoprotein precursor with foreign sequence and would result in a chimeric protein that maintained the authentic 23 N-terminal residues of Gc and should ensure correct proteolytic cleavage between NSm and the chimeric Gc protein. Therefore, we inserted the coding sequence for either eGFP or mCherry fluorescent proteins into pT7riboBUNM(+) (Fig. 1) and recovered two recombinant viruses (designated rBUNGc-eGFP and rBUNGc-mCherry) by reverse genetics (22). In BHK-21 cells, both recombinant viruses formed smaller plaques than those of wt BUNV or the Gc deletion virus rBUNGcΔ7 (Fig. 2A). The growth characteristics of the viruses were compared in BHK-21 cells infected at a low MOI (0.1 PFU/cell) at 37°C. In accord with their smaller plaque sizes, both recombinant viruses grew more slowly and to lower titers than wt BUNV (Fig. 2B), with rBUNGc-eGFP virus being more attenuated (100-fold lower titer than wt BUNV) than rBUNGc-mCherry (10-fold lower titer than wt BUNV).

The supernatant of infected cells was clarified by centrifugation to remove cellular debris, and virus particles in the clarified supernatant showed bright autofluorescence under the fluorescence microscope because every copy of the estimated 650 Gc molecules per viron (29) carried a fluorescent protein moiety (Fig. 2C). Variation in size of the fluorescent dots in both the rBUNGc-eGFP ("green virus"; left panel) and rBUNGc-mCherry ("red virus"; middle panel) viruses was noticeable, suggesting that the larger dots may represent aggregated particles. When the red and green viruses were mixed, evidence for aggregation was noted, as indicated by the yellow signal enlarged in the right-hand panel.

Characterization of chimeric Gc proteins. The proteins synthesized by the recombinant viruses were analyzed by immunoprecipitation of radiolabeled cell extracts (Fig. 3A). The size of Gc in both recombinant viruses was larger than that of the

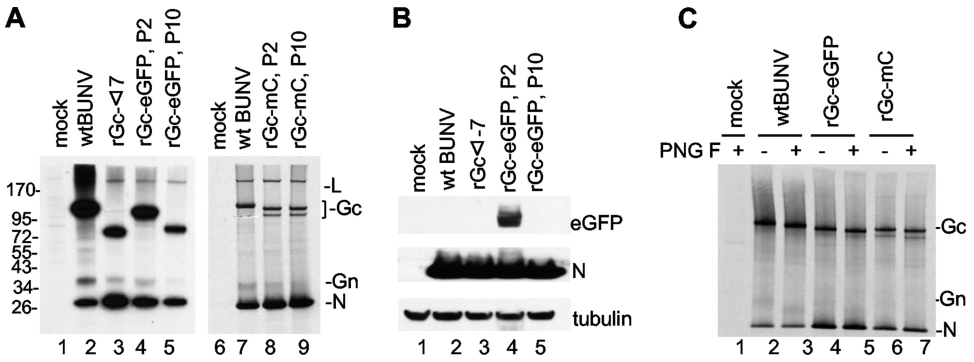

FIG. 3. Characterization of recombinant BUNV expressing chimeric Gc proteins. (A) Comparison of protein profiles of the recombinant viruses rBUNGc-eGFP (rGc-eGFP), rBUNGc-mCherry (rGc-mC), rBUNGcΔ7 (rGcΔ-7), and wt BUNV. BHK-21 cells were infected with wt or mutant viruses at an MOI of 1.0 PFU/cell or were mock infected, and cells were then labeled with [^{35}S]methionine at 24 h postinfection. Viral proteins were precipitated with anti-BUN antibodies and analyzed on 4 to 12% polyacrylamide NuPAGE gels (Invitrogen) under reducing conditions. The positions of viral proteins and protein molecular mass markers are indicated. (B) Western blot analysis to detect eGFP. BHK-21 cells were infected with wt BUNV, rBUNGcΔ7, or rBUNGc-eGFP stock from passage 2 (P2) or passage 10 (P10) or mock infected, as indicated, and cell lysates were fractionated by SDS-PAGE. After transfer to PVDF membrane, the blots were probed with anti-GFP, anti-N, and anti-tubulin antibodies as shown. (C) Glycosylation analysis of viral Gc proteins. Radiolabeled viral proteins were immunoprecipitated with anti-BUN antibodies, and then precipitates were subjected to digestion with PNGase F (F), as indicated, before fractionation on 4 to 12% polyacrylamide NuPAGE gels (Invitrogen) under reducing conditions. The positions of viral proteins are indicated.

truncated Gc produced by rBUNGcΔ7 (Fig. 3A). In cells infected by rBUNGc-mCherry, the chimeric Gc appeared as a doublet, with the slower-migrating band more dominant than the faster one (Fig. 3A, lanes 8 and 9). In the case of rBUNGc-eGFP, the presence of eGFP sequences in virus-infected cells was confirmed by Western blotting with anti-GFP antibody (Fig. 3B, lane 4).

To investigate whether the two bands corresponding to the chimeric Gc-mCherry protein arose due to differences in their N-linked glycosylation states, [^{35}S]methionine-labeled viral proteins were immunoprecipitated and subjected to PNGase F digestion. As seen in Fig. 3C, both forms of the Gc protein (lanes 6 and 7) decreased in size, indicating that the second band was not the result of differential N-linked glycosylation. As there is only one N-linked glycosylation site present on the Gc proteins expressed by rBUNGc-eGFP and rBUNGc-mCherry, the shift of size after the deglycosylation is smaller than that of wt BUNV (lanes 2 and 3) that contains two N-glycosylation sites. The genesis of the second Gc band in rBUNGc-mCherry has not been investigated further, but the pattern of bands remains consistent through repeated passages of the virus (see below).

Stability of the eGFP- and mCherry-tagged recombinant viruses. Upon passage of rBUNGc-eGFP in BHK cells, it was noted that some of the plaques produced by the virus no longer fluoresced under UV light. The number of fluorescent plaques in diluted samples of the different virus passages was assessed and showed that the percentage of fluorescent plaques decreased from 100% (12/12 plaques) at passage 5 to 46% (5/11 plaques) at passage 6 and to 0% (0/12 plaques) at passage 7 (data not shown). To investigate this loss of fluorescence, cells were infected with virus from sequential passages, and viral proteins were analyzed by immunoprecipitation and SDS-PAGE. As seen in Fig. 4A, faster-migrating bands appeared below the Gc-eGFP bands by passages 2 to 4 and increased in intensity over passages 5 and 6. At passage 6, the Gc-eGFP band showed decreased intensity, and at passage 7 no band corresponding to Gc-eGFP was detectable. A single smaller band was evident at passages 7 and 8 and appeared to be a stable species up to passage 9. The loss of eGFP sequences in virus at passage 10 was confirmed by Western blotting, where no reactivity was observed with the anti-GFP antibody (Fig. 3B, lane 5), and by cDNA sequence analysis of the M segment of the mutant viruses (see below).

In contrast to the observation for rBUNGc-eGFP, no loss of fluorescence was observed in cells infected by rBUNGc-mCherry over 10 passages (data not shown). Protein profile analysis revealed that the banding pattern of the doublet Gc protein was constant in cells infected with virus from different passages, and no smaller species were generated (Fig. 4B). Furthermore, the relative intensities of the two bands were constant across all passages. These data indicate that the chimeric Gc-mCherry protein was more stable than the Gc-eGFP protein.

The protein data suggested that rBUNGc-eGFP had deleted the eGFP coding sequence over sequential passages. Therefore, we determined the nucleotide sequence of the M genome segment of recombinant virus at passage 9 by reverse transcription-PCR (RT-PCR), which revealed that not only the complete eGFP coding region was lacking but also the upstream region coding for the remaining 23 residues at the N terminus of Gc (residues 477 to 499 in the precursor) as well as that encoding the C-terminal 135 residues of NSm (residues 342 to 476) (Fig. 4C). It should be noted that the N-terminal 39 amino acid residues of NSm (residues 303 to 341 in the precursor) were retained; these are highly conserved among different orthobunyaviruses and previously were shown to be required for replication of BUNV and the related MAGV (33, 42). Hence, in all subsequent experiments, only early-passage stocks of rBUNGc-eGFP were used, prepared as described in Materials and Methods. As also shown in Fig. 4C, the deletion of the eGFP coding region and part of NSm in the M segment of rBUNGc-eGFP is reminiscent of the internal deletion found in the M segment of the non-temperature-sensitive (ts) revertant

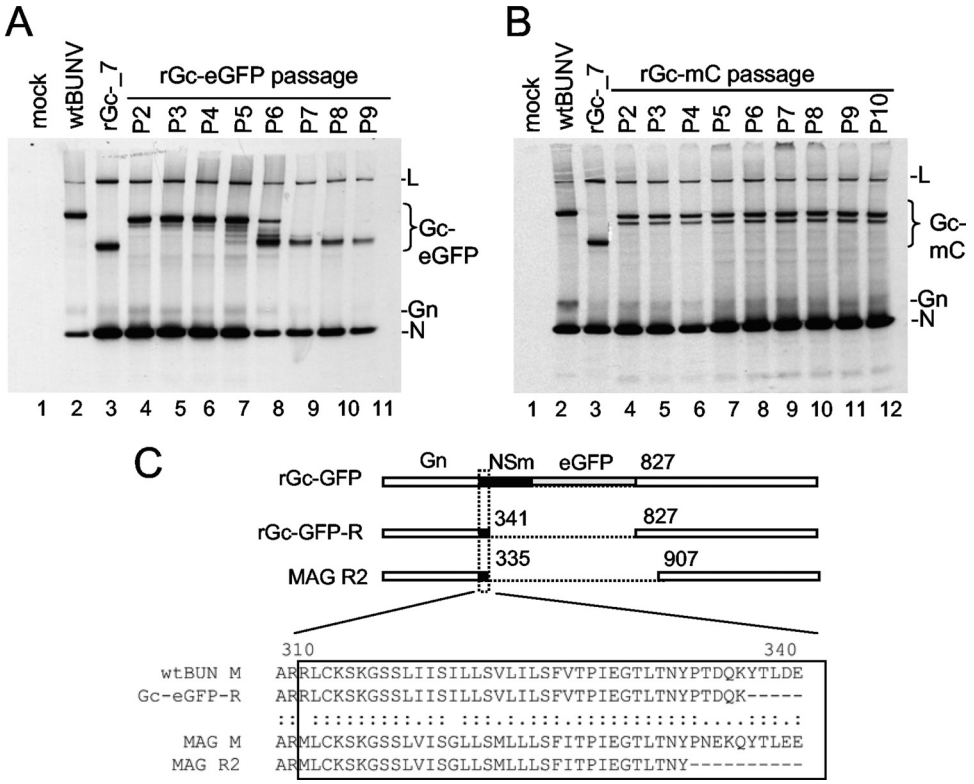

FIG. 4. Stability of fluorescent protein-tagged Gc in recombinant viruses. (A and B) Protein analysis. BHK-21 cells were infected with wt BUNV, rBUNGcΔ7, and stocks of rBUNGc-eGFP (rGc-eGFP) or rBUNGc-mCherry (rGc-mC) from passages 2 to 9 or 10, as indicated, at an MOI of 1.0 PFU/cell and labeled with [^{35}S]methionine at 24 h postinfection. Viral proteins were precipitated with anti-BUN antibodies and analyzed on 4 to 12% polyacrylamide NuPAGE gels (Invitrogen) under reducing conditions. The positions of viral proteins are indicated. (C) Sequence analysis. Alignment of the deduced amino acid sequences of the NSm-Gc region from wt BUNV, rBUNGc-eGFP passage 9, wt MAGV, and MAGV R2. Above is shown a schematic of this region, with amino acid positions indicated.

R2 virus derived from MAGV (33). Sequence analysis of the M segments of early and late passages of rBUNGc-mCherry revealed no nucleotide differences (data not shown), in accord with the stability of the protein profiles shown in Fig. 4B.

Visualization of BUNV attachment, assembly, budding, and release. The creation of fluorescent protein-tagged viruses enabled us to visualize virus infection at different stages of the life cycle, including attachment, intracellular trafficking, assembly, and budding. To observe the earliest events of virus infection, BHK-21 cells were incubated with rBUNGc-eGFP for different time periods up to 60 min at 37°C, and then the cells were washed with cold PBS and fixed with 4% paraformaldehyde. To observe later replication events, cells were infected for 60 min and washed, and incubation continued at 37°C as indicated in Fig. 5A. After fixation, the infected cells were counterstained with CellMask Deep Red Plasma Membrane Stain (Invitrogen) prior to confocal examination. As shown in Fig. 5A, virus particles were found attached to the cell surface after a 10-min incubation. Green virus particles were visible both on the cell surface and within the cytoplasm up to 4 h after initial infection though no new viral glycoprotein synthesis was apparent. By 5 h postinfection, the Golgi complex began to show evidence of nascent viral glycoprotein and discrete fluorescent spots could be observed from 6 h postinfection (Fig. 5A, panels 6 h and later). We interpret these spots as representing progeny virus particles in Golgi complex-derived vesicles, in accord with electron microscopy (EM) observations of infected cells that revealed vesicles containing single or very few (three to four) particles (28).

Bunyaviruses assemble and bud at the membranes of the Golgi complex and then must be transported through the cytoplasm for release from cell. Figure 5B shows a BSR-T7/5 cell infected with rBUNGc-eGFP at 8 h postinfection. Enlarged sections 1 and 3 show virus particles trafficking within the cell and being released at the cell surface, and section 2 shows the "factory" in the Golgi complex where viruses bud and assemble. Based on their sizes, which are identical to those of extracellular particles, most of the intracellular virus particles appear to be individual virions rather than aggregates. In enlarged section 3, some virus particles are seen in close association with, or on the tips of, microtubules, perhaps indicating the involvement of microtubules in the intracellular trafficking and release of virions.

Figure 6 shows the Golgi complex in cells infected with wt BUNV or rBUNGc-eGFP. In both cases the Golgi complex was identified by staining with an antibody to the Golgi complex marker GM130, and colocalization of Gc with this organelle is shown by yellow in the merged images (Fig. 6C and G). In Fig. 6C, the Gc protein was stained with MAb 742, a Gc-specific monoclonal antibody (18). In Fig. 6G and the enlarged image in panel H, green virus particles in cells infected with rBUNGc-eGFP virus were shown both in the cytoplasm

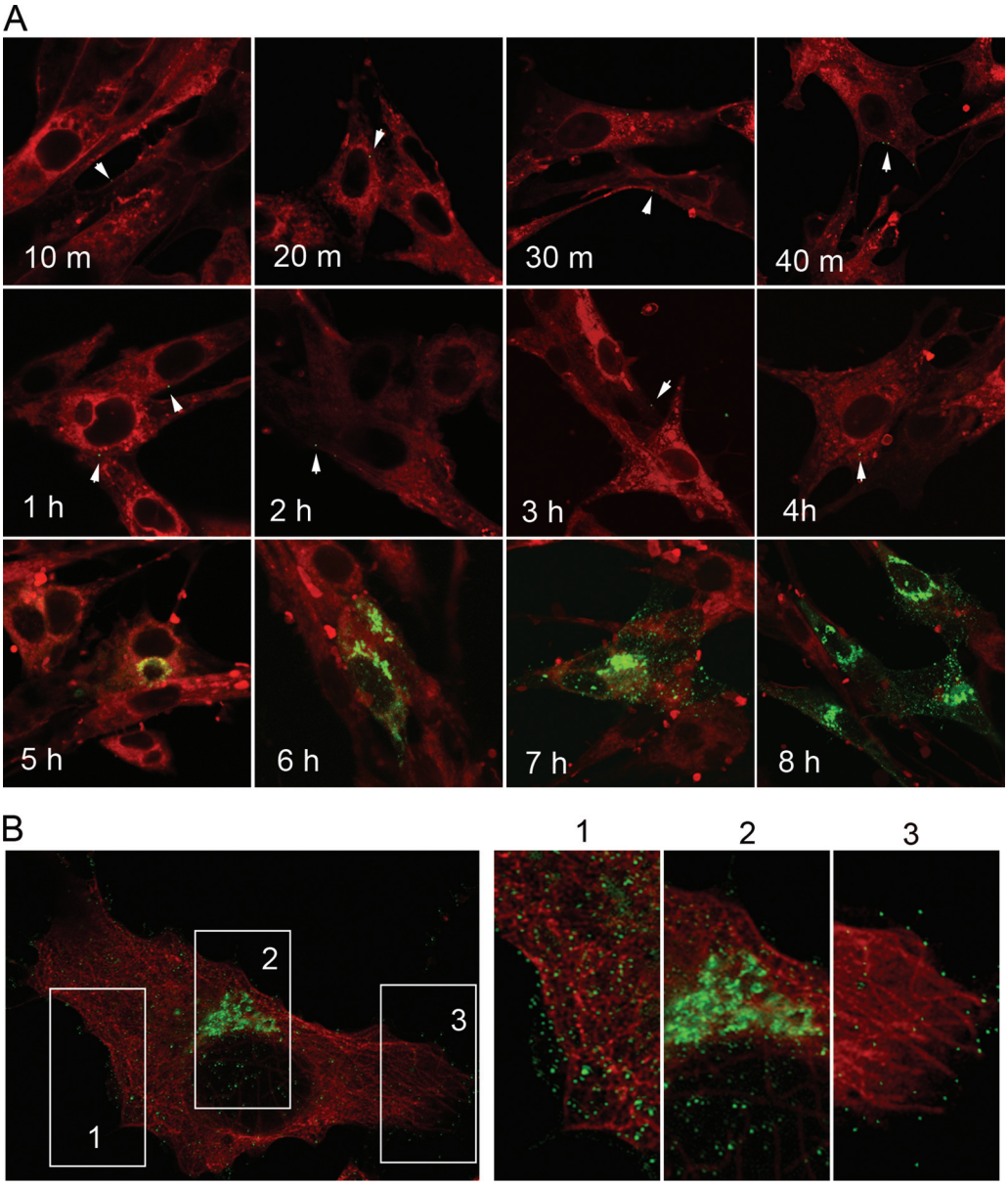

FIG. 5. Time course of rBUNGc-eGFP infection. (A) BHK-21 cells were infected with rBUNGc-eGFP at an MOI of 1 PFU/cell and incubated at 37°C for 10 min to 8 h, as indicated, prior to fixation with 4% paraformaldehyde. Cells were counterstained in red with CellMask Deep Red Plasma Membrane Stain (Invitrogen). Representative green virus particles that were either attached to or internalized into the cells at early stages of infection (1 h to 4 h) are marked by arrows though in some cells multiple particles can be seen attached. (B) BSR-T7/5 cells were infected for 8 h with rBUNGc-eGFP at an MOI of 1 PFU/cell, fixed, and costained with anti-tubulin antibody (in red). Enlarged images of selected regions 1, 2, and 3 show progeny virus particles and the virus assembly site as described in the text.

and at membranes of the Golgi complex (Fig. 6 E to H). However, no individual virus particles could be detected by staining with MAb 742 (enlarged image in Fig. 6D). It is likely that MAb 742 may not recognize Gc proteins that have already been packed icosahedrally into the virion envelope, perhaps due to conformational alteration of the glycoproteins in assembled particles or spatial hindrance for access of the antibody to the epitope, which is conformational and located at or near the first glycosylation site on Gc (residue 424) (38).

Morphological changes to the Golgi complex in BUNV-infected cells. BUNV infection of African green monkey-derived Vero cells results in early fragmentation of the Golgi complex (34). Using the fluorescent protein-tagged viruses, we investigated Golgi complex disruption in cells derived from other species. Cells were infected at a low MOI in order to allow viewing of infected and uninfected cells in the same microscopic field, and as shown in Fig. 7A to H, changes to Golgi complex morphology were also observed in human (A549)- and rodent (BHK and BSR-T7/5)-derived cells though to a lower degree than in Vero cells that were included as a control. For these investigations, the Golgi complex was stained with an antibody to GM130, and we reconstructed 3D images of the

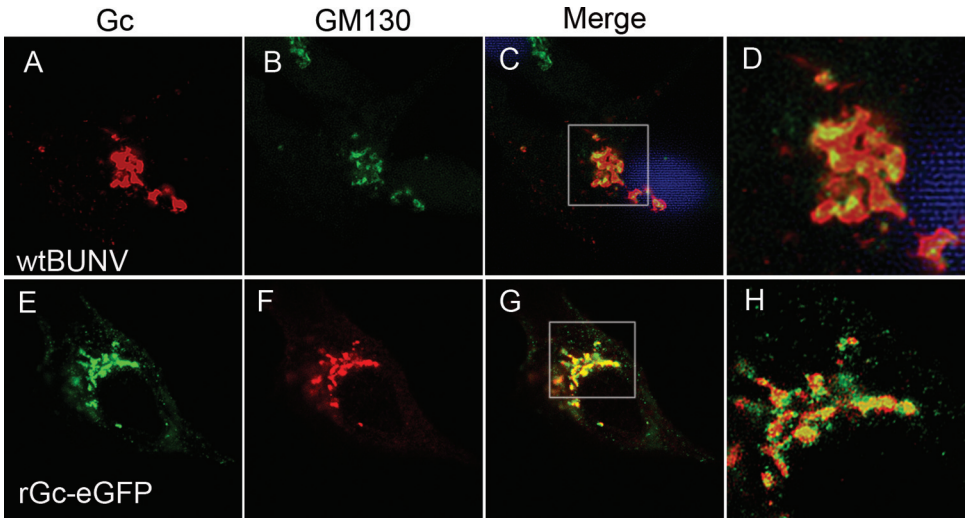

FIG. 6. Visualization of virus budding at the Golgi complex. BSRT7/5 cells were infected with either wt BUNV (A to D) or rBUNGc-eGFP (E to H) and costained with antibodies to the Golgi marker GM130 (red). BUNV Gc protein in wt BUNV-infected cells was detected with BUNV Gc-specific MAb742. Colocalization between Gc proteins and the Golgi protein are shown in yellow in the merged images (C and G), and enlarged images are shown in panels D and H.

green or red recombinant virus-infected cells from *Z*-stack images obtained by Deltavision restoration microscopy using deconvolution and surface rendering software, as described in Materials and Methods. The Golgi structures in uninfected cells (indicated by asterisks in Fig. 7A to H) were relatively compact, whereas in infected cells the Golgi complex, modified by the insertion of Gc protein, appeared rather expanded or dispersed (indicated by solid arrows). These observations suggest that Golgi complex disruption is a ubiquitous effect on cell structure caused by BUNV infection though the extent differs between different cell types. Figure 7I to L show a time course of Golgi complex disruption in BHK-21 cells infected with rBUNGc-eGFP. Changes in morphology were first seen at 6 h postinfection, and Golgi complexes were completely disrupted by 12 h postinfection. This timescale is much later than that seen in Vero cells, where fragmentation is observed before the detection of viral glycoprotein (34).

Live-cell imaging of fluorescent protein-tagged BUNV infection. To visualize the viral replication cycle in real time, BHK-21 cells grown in chamber slides were infected with rBUNGc-eGFP and incubated at 33°C in an environmental chamber on the Deltavision restoration microscope. In this situation, which includes using CO_2-independent growth medium, BUNV replication proceeds considerably more slowly than under standard growth conditions (unpublished data). Images were taken at 10-min intervals from 12 h p.i.; Fig. 8 shows only the images taken at hourly intervals (for the complete video clip, see Video S1 in the supplemental material). Fluorescent virus particles were seen trafficking from the assembly site in the Golgi region to the cell surface up to 21 h p.i. The dynamic live-cell imaging also revealed the morphological change in the Golgi complex from a tightly packed structure to a loose and fragmented structure from 13 h to 16 h p.i. (based on the colocalization with the fluorescent Gc protein). Also noteworthy is the formation of a dense fluorescent mass which we think is most likely accumulation of misfolded glycoproteins in the Golgi region from 17 h p.i. BUNV replication induces apoptosis at late stages of infection (15), and this is visualized as the collapse of the infected cell between 21 and 22 h p.i.

DISCUSSION

The N-terminal half of the Gc ectodomain of BUNV was previously shown to be dispensable for virus replication in cell culture (41). Two "fluorescent" viruses were generated by replacing 346 amino acid residues at the N terminus of Gc with either eGFP or mCherry fluorescent proteins. The viability and autofluorescence of recombinant viruses indicated that both chimeric Gc proteins were functional and could fold correctly. Though the recombinant viruses were attenuated in cell culture, they were competent to infect as wide a range of cell lines as wt BUNV (results not shown) and were able to produce workable virus yields of 5×10^6 PFU/ml. The recombinant fluorescently tagged viruses are thus valuable reagents with which to study virus entry, assembly, intracellular trafficking, and egress, as well as interactions with the host cell.

Recent electron tomographic studies of RVFV and Uukuniemi virus (UUKV) particles (both members of the *Phlebovirus* genus in the bunyavirus family) revealed that the spikes on the virion surface comprise 720 copies of each glycoprotein, Gn and Gc, arranged in an icosahedral lattice (T=12) (9, 30, 37). It is suggested that this feature might be shared by all the viruses in the family (9, 37) and thus accounts for the intense autofluorescence observed with the recombinant viruses (Fig. 2). It is perhaps remarkable that such a simple virion can accommodate this gross perturbation and retain viability compared to other viruses that have been created with fluorescent protein-tagged components which have more complex virion structures, for example, vaccinia virus (47), coronavirus (1), amphotropic retrovirus 4070A (46), herpes simplex virus (HSV) (21), and rabies virus (14).

Whereas rBUNGc-mCherry was quite stable upon repeated

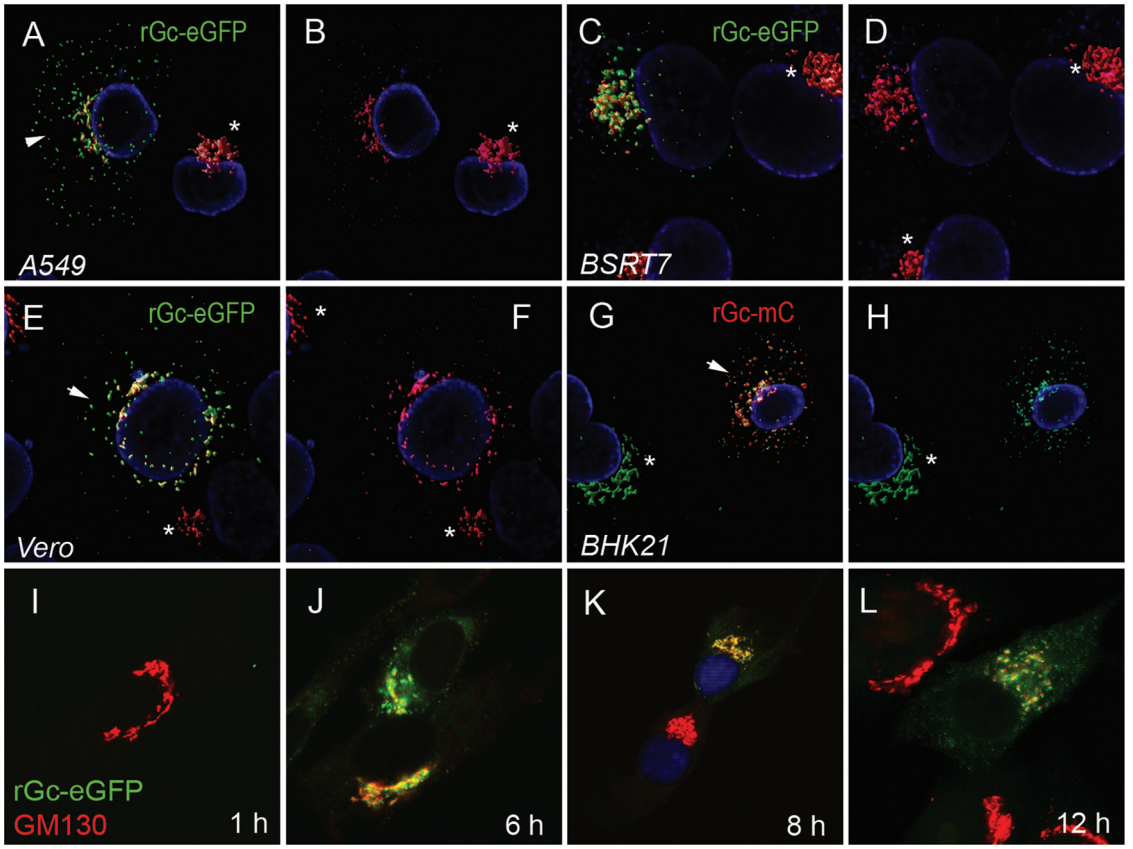

FIG. 7. Morphological changes to the Golgi complex in BUNV-infected cells. A549 (A and B), BSR-T7/5 (C and D), Vero (E and F), and BHK-21 (G and H) cells were infected with either rBUNGc-eGFP (A to F) or rBUNGc-mCherry (G and H). After fixation, cells were stained with anti-GM130 antibodies to detect the Golgi complex, and 3D images were reconstructed from *Z*-stack images using Huygens deconvolution and surface rendering software. The Golgi complexes in uninfected cells are marked with an asterisk, and those in infected cells are indicated with an arrow. Nuclei were stained in blue with 4′,6′-diamidino-2-phenylindole (DAPI). Panels I to L show the time course of Golgi complex disruption in BSR-T7/5 cells infected with rBUNGc-eGFP. Cells were fixed at 1, 6, 8, and 12 h postinfection, and the Golgi complex was stained in red with antibodies to GM130.

passage, rBUNGc-eGFP was less stable and shed the eGFP coding region after six passages. It is intriguing that deletion of the eGFP sequence was accompanied by the loss of the C-terminal 135 residues of the NSm protein (78% of NSm was lost, and only the N-terminal 39 residues of NSm remained). This is reminiscent of the generation of the non-temperature-sensitive (ts) revertant R2 of MAGV from its mutant ts8. MAGV ts8 has three amino acid substitutions in the N-terminal domain of Gc compared to the sequence of wt MAGV. In MAGV R2, the N-terminal 431 residues of Gc together with the C-terminal 130 residues of NSm were deleted (33). However, in both cases, the conserved N-terminal 39 residues of NSm were retained, further confirming the crucial requirement of these residues in viral replication (33, 42). It also illustrates the remarkable plasticity of the orthobunyavirus glycoprotein gene, and it will be of interest to determine the mechanism by which the sequences are deleted. The instability of the eGFP-tagged Gc chimera may be related to possible disulfide formation between the eGFP and Gc domains. Both Gn and Gc glycoproteins are cysteine-rich integral transmembrane proteins that mature in the lumens of the ER and Golgi complex. It has been reported that the two cysteine residues of eGFP might form disulfide-bonded oligomers (12), but perhaps these residues could form inappropriate disulfide bonds with those of Gn and or Gc protein, resulting in misfolding. This requires further investigation. In contrast, the mCherry protein does not contain cysteine residues and matures more quickly than eGFP (36). Indeed, we noticed that the rBUNGc-eGFP virus grows more slowly than rBUNGc-mCherry, and this may be related to the rate of the chimeric glycoprotein maturation.

Entry of many enveloped viruses is initiated by the attachment of viral spike glycoproteins to molecules on the plasma membrane of target cells, followed by receptor-mediated endocytosis (25, 45). Using the autofluorescent recombinant viruses, attachment and internalization of BUNV particles were clearly visualized at the early stage of virus infection, within 10 min of incubation, and by live-cell imaging we recorded steps in virus budding and egress. Most bunyaviruses assemble and bud at the membrane of the Golgi complex though details of these processes have yet to be clarified. The initial formation of virus particles must take place by curving of the viral glycoprotein-embedded Golgi membrane inward toward the lumen of the organelle (inward budding) (28, 34), followed by outward budding of mature virus particles from the Golgi lumen. The outward budding at the Golgi membranes was evident in rBUNGc-eGFP-infected cells, and it was obvious that most of

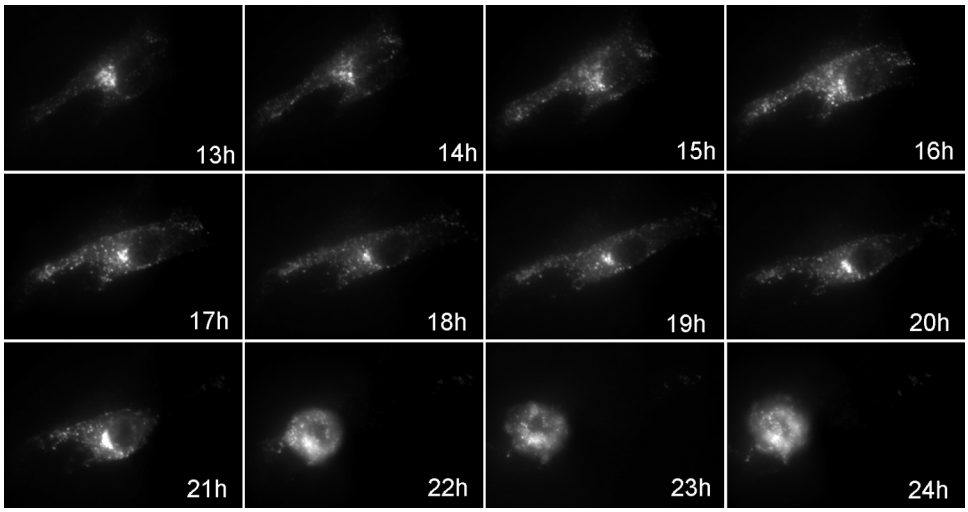

FIG. 8. Live-cell imaging of BHK-21 cells infected with rBUNGc-eGFP. BHK-21 cells grown on microscope chamber slides were infected with rBUNGc-eGFP at an MOI of 1 PFU/cell and incubated at 33°C in an environmental chamber mounted on the Deltavision restoration microscope. Images were collected at 10-min intervals from 12 h postinfection with a *Z*-section setting of 1 μm (11 images from top to bottom of the cell). Images taken at each hour are shown in the figure (for the complete video clip, see Video S1 in the supplemental material).

the virus particles transported individually instead of as a bigger cargo to the cell surface. Perhaps the intracellular trafficking of virus particles is similar to the trafficking of post-Golgi transport carriers (PGCs), dynamic and membrane-bound organelles (24), which is promoted by cytoskeletal elements, particularly microtubules and associated motor proteins (23). We noticed contact between green virus particles and microtubules in infected cells, suggesting involvement of cytoskeleton proteins in virus trafficking. However, we did not observe the tubule-like structures arising from membranes of the Golgi complex in BUNV-infected cells that are characteristic in the morphogenesis of PGCs (23, 32).

BUNV infection of Vero cells leads to early Golgi complex fragmentation in Vero cells, before the detection of viral glycoproteins (34). Our results demonstrated that infection-induced Golgi complex disruption is not limited to Vero cells but is common to other cell types though it occurs later in infection, probably due to the segregation or redistribution of the integral Golgi proteins caused by the accumulation of viral glycoproteins or virus assembly and budding itself. Studies of UUKV-infected BHK-21 cells showed that infection caused expansion and vacuolization of the Golgi complex though the disrupted Golgi complex was still functional in its ability to glycosylate and transport glycoproteins destined for the plasma membrane (10). Furthermore, BUNV infection can cause cell death (15), and Golgi complex fragmentation might be a cellular response due to apoptosis (17, 26).

As the recombinant BUNVs exhibit strong autofluorescence, we anticipate that they will be excellent candidates for the application of advanced microscopical and single-particle tracking techniques that have been used for visualizing infection by other enveloped viruses such influenza, vesicular stomatitis, and human immunodeficiency viruses (2, 5, 13, 16). Such studies will reveal further details of the BUNV infection cycle.

ACKNOWLEDGMENTS

We thank John Nicholson for assistance with live-cell imaging.

Work in R.M.E.'s laboratory is funded by grants from the Wellcome Trust, MRC, and BBSRC.

REFERENCES

1. **Bosch, B. J., C. A. M. de Haan, and P. J. M. Rottier.** 2004. Coronavirus spike glycoprotein, extended at the carboxy terminus with green fluorescent protein, is assembly competent. J. Virol. **78:**7369–7378.
2. **Brandenburg, B., and X. Zhuang.** 2007. Virus trafficking—learning from single-virus tracking. Nat. Rev. Microbiol. **5:**197–208.
3. **Bridgen, A., and R. M. Elliott.** 1996. Rescue of a segmented negative-strand RNA virus entirely from cloned complementary DNAs. Proc. Natl. Acad. Sci. U. S. A. **93:**15400–15404.
4. **Buchholz, U. J., S. Finke, and K. K. Conzelmann.** 1999. Generation of bovine respiratory syncytial virus (BRSV) from cDNA: BRSV NS2 is not essential for virus replication in tissue culture, and the human RSV leader region acts as a functional BRSV genome promoter. J. Virol. **73:**251–259.
5. **Cureton, D. K., R. H. Massol, S. Saffarian, T. L. Kirchhausen, and S. P. J. Whelan.** 2009. Vesicular stomatitis virus enters cells through vesicles incompletely coated with clathrin that depend upon actin for internalization. PLoS Pathog. **5:**e1000394.
6. **Elliott, R., M. Bouloy, C. H. Calisher, R. Goldbach, J. T. Moyer, S. T. Nichol, R. Pettersson, A. Plyusnin, and C. S. Schmaljohn.** 2000. *Bunyaviridae*, p. 599–621. *In* M. H. V. van Regenmortel, C. M. Fauquet, D. H. L. Bishop, E. B. Carstens, M. K. Estes, S. M. Lemon, J. Maniloff, M. A. Mayo, D. J. McGeoch, C. R. Pringle, and E. B. Wickner (ed.), Virus taxonomy: classification and nomenclature of viruses. Seventh report of the International Committee on Taxonomy of Viruses. Academic Press, San Diego, CA.
7. **Elliott, R. M.** 1997. Emerging viruses: the *Bunyaviridae*. Mol. Med. **3:**572–577.
8. **Elliott, R. M.** 1990. Molecular biology of the *Bunyaviridae*. J. Gen. Virol. **71:**501–522.
9. **Freiberg, A. N., M. B. Sherman, M. C. Morais, M. R. Holbrook, and S. J. Watowich.** 2008. Three-dimensional organization of Rift Valley fever virus revealed by cryoelectron tomography. J. Virol. **82:**10341–10348.
10. **Gahmberg, N., R. F. Pettersson, and L. Kääriäinen.** 1986. Efficient transport of Semliki Forest virus glycoproteins through a Golgi complex morphologically altered by Uukuniemi virus glycoproteins. EMBO J. **5:**3111–3118.
11. **Heim, R., A. B. Cubitt, and R. Y. Tsien.** 1995. Improved green fluorescence. Nature **373:**663–664.
12. **Jain, R. K., P. B. Joyce, M. Molinete, P. A. Halban, and S. U. Gorr.** 2001. Oligomerization of green fluorescent protein in the secretory pathway of endocrine cells. Biochem. J. **360:**645–649.
13. **Jouvenet, N., P. D. Bieniasz, and S. M. Simon.** 2008. Imaging the biogenesis of individual HIV-1 virions in live cells. Nature **454:**236–240.

14. **Klingen, Y., K.-K. Conzelmann, and S. Finke.** 2008. Double-labeled rabies virus: live tracking of enveloped virus transport. J. Virol. **82:**237–245.
15. **Kohl, A., R. F. Clayton, F. Weber, A. Bridgen, R. E. Randall, and R. M. Elliott.** 2003. Bunyamwera virus nonstructural protein NSs counteracts interferon regulatory factor 3-mediated induction of early cell death. J. Virol. **77:**7999–8008.
16. **Lakadamyali, M., M. J. Rust, H. P. Babcock, and X. Zhuang.** 2003. Visualizing infection of individual influenza viruses. Proc. Natl. Acad. Sci. U. S. A. **100:**9280–9285.
17. **Lane, J. D., J. Lucocq, J. Pryde, F. A. Barr, P. G. Woodman, V. J. Allan, and M. Lowe.** 2002. Caspase-mediated cleavage of the stacking protein GRASP65 is required for Golgi fragmentation during apoptosis. J. Cell Biol. **156:**495–509.
18. **Lappin, D. F., G. W. Nakitare, J. W. Palfreyman, and R. M. Elliott.** 1994. Localization of Bunyamwera bunyavirus G1 glycoprotein to the Golgi requires association with G2 but not with NSm. J. Gen. Virol. **75:**3441–3451.
19. **Lees, J. F., C. R. Pringle, and R. M. Elliott.** 1986. Nucleotide sequence of the Bunyamwera virus M RNA segment: conservation of structural features in the Bunyavirus glycoprotein gene product. Virology **148:**1–14.
20. **Leonard, V. H., A. Kohl, J. C. Osborne, A. McLees, and R. M. Elliott.** 2005. Homotypic interaction of Bunyamwera virus nucleocapsid protein. J. Virol. **79:**13166–13172.
21. **Lorentzen, E. U., B. R. Eing, W. Hafezi, R. Manservigi, and J. E. Kçhn.** 2001. Replication-competent herpes simplex virus type 1 mutant expressing an autofluorescent glycoprotein H fusion protein. Intervirology **44:**232–242.
22. **Lowen, A. C., C. Noonan, A. McLees, and R. M. Elliott.** 2004. Efficient bunyavirus rescue from cloned cDNA. Virology **330:**493–500.
23. **Luini, A., A. Mironov, E. Polishchuk, and R. Polishchuk.** 2008. Morphogenesis of post-Golgi transport carriers. Histochem. Cell Biol. **129:**153–161.
24. **Luini, A., A. Ragnini-Wilson, R. S. Polishchuck, and M. A. D. Matteis.** 2005. Large pleiomorphic traffic intermediates in the secretory pathway. Curr. Opin. Cell Biol. **17:**353–361.
25. **Marsh, M., and A. Helenius.** 2006. Virus entry: open sesame. Cell **124:**729–740.
26. **Mukherjee, S., R. Chiu, S.-M. Leung, and D. Shields.** 2007. Fragmentation of the Golgi apparatus: an early apoptotic event independent of the cytoskeleton. Traffic **8:**369–378.
27. **Nichol, S. T., B. Beaty, R. M. Elliott, R. Goldbach, A. Plyusnin, A. L. Schmaljohn, and R. B. Tesh.** 2005. Bunyaviridae, p. 695–716. *In* C. M. Fauquet, M. A. Mayo, J. Maniloff, U. Desselberger, and L. A. Ball (ed.), Virus taxonomy: classification and nomenclature of viruses. Eighth report of the International Committee on Taxonomy of Viruses. Elsevier/Academic Press, London, United Kingdom.
28. **Novoa, R. R., G. Calderita, P. Cabezas, R. M. Elliott, and C. Risco.** 2005. Key Golgi factors for structural and functional maturation of Bunyamwera virus. J. Virol. **79:**10852–10863.
29. **Obijeski, J. F., D. H. Bishop, F. A. Murphy, and E. L. Palmer.** 1976. Structural proteins of La Crosse virus. J. Virol. **19:**985–997.
30. **Overby, A. K., R. F. Pettersson, K. Grunewald, and J. T. Huiskonen.** 2008. Insights into bunyavirus architecture from electron cryotomography of Uukuniemi virus. Proc. Natl. Acad. Sci. U. S. A. **105:**2375–2379.
31. **Pettersson, R. F., and L. Melin.** 1996. Synthesis, assembly, and intracellular transport of Bunyaviridae membrane proteins, p. 159–188. *In* R. M. Elliott (ed.), The *Bunyaviridae*. Plenum Press, New York, NY.
32. **Polishchuk, E. V., A. Di Pentima, A. Luini, and R. S. Polishchuk.** 2003. Mechanism of constitutive export from the Golgi: bulk flow via the formation, protrusion, and en bloc cleavage of large *trans*-Golgi network tubular domains. Mol. Biol. Cell **14:**4470–4485.
33. **Pollitt, E., J. Zhao, P. Muscat, and R. M. Elliott.** 2006. Characterization of Maguari orthobunyavirus mutants suggests the nonstructural protein NSm is not essential for growth in tissue culture. Virology **348:**224–232.
34. **Salanueva, I. J., R. R. Novoa, P. Cabezas, C. Lopez-Iglesias, J. L. Carrascosa, R. M. Elliott, and C. Risco.** 2003. Polymorphism and structural maturation of Bunyamwera virus in Golgi and post-Golgi compartments. J. Virol. **77:**1368–1381.
35. **Schmaljohn, C., and J. W. Hooper.** 2001. Bunyaviridae: the viruses and their replication, p. 1581–1602. *In* B. N. Fields, D. M. Knipe, P. M. Howley, D. E. Griffin, R. A. Lamb, M. A. Martin, B. Roizman, and S. E. Straus (ed.), Fields virology, 4th ed. Lippincott Williams & Wilkins, Philadelphia, PA.
36. **Shaner, N. C., R. E. Campbell, P. A. Steinbach, B. N. Giepmans, A. E. Palmer, and R. Y. Tsien.** 2004. Improved monomeric red, orange and yellow fluorescent proteins derived from *Discosoma* sp. red fluorescent protein. Nat. Biotechnol. **22:**1567–1572.
37. **Sherman, M. B., A. N. Freiberg, M. R. Holbrook, and S. J. Watowich.** 2009. Single-particle cryo-electron microscopy of Rift Valley fever virus. Virology **387:**11–15.
38. **Shi, X., K. Brauburger, and R. M. Elliott.** 2005. Role of N-linked glycans on Bunyamwera virus glycoproteins in intracellular trafficking, protein folding, and virus infectivity. J. Virol. **79:**13725–13734.
39. **Shi, X., and R. M. Elliott.** 2004. Analysis of N-linked glycosylation of Hantaan virus glycoproteins and the role of oligosaccharide side chains in protein folding and intracellular trafficking. J. Virol. **78:**5414–5422.
40. **Shi, X., and R. M. Elliott.** 2002. Golgi localization of Hantaan virus glycoproteins requires coexpression of G1 and G2. Virology **300:**31–38.
41. **Shi, X., J. Goli, G. Clark, K. Brauburger, and R. M. Elliott.** 2009. Functional analysis of the Bunyamwera orthobunyavirus Gc glycoprotein. J. Gen. Virol. **90:**2483–2492.
42. **Shi, X., A. Kohl, V. Léonard, P. Li, A. McLees, and R. Elliott.** 2006. Requirement of the N-terminal region of the orthobunyavirus non-structural protein NSm for virus assembly and morphogenesis. J. Virol. **80:**8089–8099.
43. **Shi, X., A. Kohl, P. Li, and R. M. Elliott.** 2007. Role of the cytoplasmic tail domains of Bunyamwera orthobunyavirus glycoproteins Gn and Gc in virus assembly and morphogenesis. J. Virol. **81:**10151–10160.
44. **Shi, X., D. F. Lappin, and R. M. Elliott.** 2004. Mapping the Golgi targeting and retention signal of Bunyamwera virus glycoproteins. J. Virol. **78:**10793–10802.
45. **Sieczkarski, S. B., and G. R. Whittaker.** 2005. Viral entry. Curr. Top. Microbiol. Immunol. **285:**1–23.
46. **Spitzer, D., K. E. Dittmar, M. Rohde, H. Hauser, and D. Wirth.** 2003. Green fluorescent protein-tagged retroviral envelope protein for analysis of virus-cell interactions. J. Virol. **77:**6070–6075.
47. **Ward, B. M., and B. Moss.** 2001. Visualization of intracellular movement of vaccinia virus virions containing a green fluorescent protein-B5R membrane rrotein chimera. J. Virol. **75:**4802–4813.
48. **Watret, G. E., C. R. Pringle, and R. M. Elliott.** 1985. Synthesis of bunyavirus-specific proteins in a continuous cell line (XTC-2) derived from *Xenopus laevis*. J. Gen. Virol. **66:**473–482.
49. **Weber, F., E. F. Dunn, A. Bridgen, and R. M. Elliott.** 2001. The Bunyamwera virus nonstructural protein NSs inhibits viral RNA synthesis in a minireplicon system. Virology **281:**67–74.